

Article

Indoor Particulate Matter Transfer in CNC Machining Workshop and The Influence of Ventilation Strategies—A Case Study

Huimin Yao ¹, Shanshan Qiu ¹, Yuling Lv ¹, Shen Wei ², Ang Li ¹, Zhengwei Long ^{1,*}, Wentao Wu ³
and Xiong Shen ^{1,*}

¹ Tianjin Key Lab of Indoor Air Environmental Quality Control, School of Environmental Science and Engineering, Tianjin University, Tianjin 300072, China

² The Bartlett School of Sustainable Construction, University College London (UCL), 1–19 Torrington Place, London WC1E 7HB, UK

³ Department of Civil and Natural Resources Engineering, University of Canterbury, Christchurch 8041, New Zealand

* Correspondence: longzw@tju.edu.cn (Z.L.); shenxiong@tju.edu.cn (X.S.); Tel.: +86-13820921056 (X.S.)

Abstract: Particulate matter in Computer Numerical Control (CNC) machining workshop is harmful to workers' health. This paper studies particulate matter transfer and the performance of various ventilation strategies in a CNC machining workshop. To obtain the boundary condition of the particle field, instruments were installed to obtain the particle size attenuation characteristics and source strength, respectively. The results show that the 99% cumulative mass concentration of particles is distributed within 1.5 μm , and the release rate of particles from the full enclosure. Next, the indoor flow field and particle field were simulated by numerical simulation with the measured boundary conditions. The working area's age of air, particle concentration, and ventilation efficiency were compared between four displacement ventilation methods and one mixed ventilation method. The results show that the working area's mean particle concentration and ventilation efficiency under longitudinal displacement ventilation is better than other methods. At the same time, the mean age of air is slightly worse. In addition, mixed ventilation can obtain lower mean age of air, but the particle concentration is higher in the working area. The bilateral longitudinal ventilation can be improved by placing axial circulation fans with vertical upward outlets in the center of the workshop.

Keywords: particle matter; machining workshop; numerical model; displacement ventilation; age of air



Citation: Yao, H.; Qiu, S.; Lv, Y.; Wei, S.; Li, A.; Long, Z.; Wu, W.; Shen, X. Indoor Particulate Matter Transfer in CNC Machining Workshop and The Influence of Ventilation Strategies—A Case Study. *Sustainability* **2023**, *15*, 6227. <https://doi.org/10.3390/su15076227>

Academic Editor: Reza Daneshazarian

Received: 20 December 2022

Revised: 11 March 2023

Accepted: 29 March 2023

Published: 4 April 2023



Copyright: © 2023 by the authors. Licensee MDPI, Basel, Switzerland. This article is an open access article distributed under the terms and conditions of the Creative Commons Attribution (CC BY) license (<https://creativecommons.org/licenses/by/4.0/>).

1. Introduction

Computer Numerical Control (CNC) of machining tools is widely used by metal manufacturing workshops to increase productivity [1]. Metalworking fluid is commonly applied to cool and lubricate metal components in CNC machining workshops, but this operation produces a large amount of hydrocarbon oil mist [2]. The concentration of oil mist is related to occupational health management due to the pathogenic tendency of metal cutting fluid and the unavoidable close contact with workshop workers [3]. Long-term exposure to oil mist of high levels of concentration may result in a severe adverse impact on people's lungs and respiratory tract and cause health issues like hypersensitivity pneumonia [4], lipoid pneumonia [5], lung cancer, laryngeal cancer [6], asthma, and hyper bronchial responsiveness [7]. Short-term exposure to oil mist impacts the operators' working performance [8]. American National Institute of Procurement Safety and Health (NIOSH) issued a Standard [9] to require Recommended Exposure Level (REL) for oil mist lower than 0.5 mg/m^3 . However, the concentration of oil mist often exceeds the limit of REL in many CNC workshops [10].

CNC workshops control the concentration of oil mist with industrial ventilation, either mixed or displacement ventilation [11]. Mixed ventilation supplies fresh air of high velocity

(>4 m/s) to the work zone to dilute the stale air polluted by oil mist [12,13]. On the contrary, displacement ventilation provides fresh air directly to the work zone at a generally lower air velocity (0.2 m/s ~ 0.5 m/s) and forms a unidirectional flow zone in the lower area of space to displace the air polluted by oil mist [14]. The placement of the ventilation and its influence on the process of removing contaminants in workshops are worthy of study [15]. The performance of mixing and displacement ventilation in controlling contaminant levels for industrial spaces has been debated for many years. Compared to mixing ventilation, displacement ventilation was reported to have a lower particle deposition rate and a larger number of escaped particles [16]. Displacement ventilation is reported to have better ventilation efficiency within the work zone [17,18] but has fewer ventilation rates compared to mixing ventilation [19]. Although recirculating air systems with roof exhausts can enhance the flow rates of displacement ventilation [20], there remain other concerns over displacement ventilation, including the resuspension of particles deposited on the ground [21] and inefficiency for tall industrial workspaces [22]. The performance of either mixing or displacement ventilation is not satisfactory in controlling the concentration of oil mist in individual work zones.

The ventilation strategies need to be optimized to efficiently remove oil mist for each machining cover operated by a worker. Wei et al. [23] proposed to furnish air from the lower part of the support columns in a machining plant and extract polluted air from the ceiling. The improved displacement ventilation system, with the aid of thermal plumes, can reduce the oil-mist concentration by 70% in the work zones. Wang et al. [24] proposed a coupled uniform push-pull ventilation and air curtain system, but the system causes serious dispersion of oil mist in the condition of high air jet velocity and low push-pull airflow rate. Despite the existing research on ventilation strategies to reduce the concentration of oil mist, knowledge is still missing on different installation positions of supply and return air outlets, the efficiency of other ventilation strategies, including single-side transverse and bilateral transverse ventilation, and especially the spatial distribution of oil mist under different ventilation schemes.

Another gap in understanding the performance of different ventilation strategies to remove oil mist is the lack of in-situ experiments [25]. It is challenging to conduct in-situ measurements in CNC workshops due to the spatial size of the oil mist. Alternatively, laboratory experiments with the reduced-scale model using water tunnels were applied [26,27]. It is challenging to achieve dynamic similarity because inertial and buoyancy forces are not comparable at the same time. Another common approach is to apply CFD to evaluate the ventilation performance in CNC workshops. CFD has been applied for the design of the proper ventilation system for a workshop, but the simulation results may not agree with on-site measurements [28]. It does not make sense to study the performance of displacement ventilation systems for large machining plants without in-situ experimental data to validate CFD results. Most of the existing research is based on models and lacks comprehensive consideration of the actual processing environment, which leads to the lack of experimental verification and reduces the credibility of the simulated result.

To address the above research gaps, this study aims to explore the differences and characteristics of several ventilation strategies, including both mixed ventilation and displacement ventilation, to guide the ventilation design for CNC workshops. The objectives include (1) carrying out in-situ experiments in a CNC workshop located in Tianjin, China, to collect detailed data on concentration and particle size; (2) developing and validating a CFD model to study the spatial distribution of oil mist under different ventilation strategies; (3) optimize ventilation strategies for CNC workshops to reduce workers' health risk.

2. Materials and Methods

2.1. In-Situ Experiments

A typical CNC machining workshop was selected as the research object in this study. The temperature and velocity in the working area of the workshop were monitored through field experiments, which were used as the boundary conditions of the CFD model and

for model validation. Additionally, the concentration of oil mist inside and outside the equipment was monitored to analyze the dispersion of fine particles.

2.1.1. Investigated CNC Workshop

The CNC machining workshop (shown in Figure 1) is located in Tianjin, China. It is 87 m long (X), 34 m wide (Z), and 6 m high (Y). The workshop mainly processes small mechanical parts, such as mobile phone parts. The equipment in the workshop is semi-automatic processing equipment, with wet cutting as the primary processing technology. Wet cutting produces many fine particles [29]. In total, 172 pieces of machining equipment are located in seven rows and divided into six zones (Zones 1–6). Each machining equipment is covered with metal enclosures installed in the workshop. The dimensions are 1.6 m (Length) \times 1.3 m (Width) \times 1.7 m (Height). During the production process, operators stay in the area between the two rows of enclosures without oil mist purification. Therefore, oil mist particles are released directly into the indoor space through the leakage area on the enclosure's walls. The leakage area includes operation doors (0.6 m \times 1.0 m) and an open ceiling (1.6 m \times 1.3 m). In each machining process, the operator opens the operation door, places the machined workpiece into the machining area, and opens the metalworking fluid. After closing the door, the workpiece will be processed automatically by the machine.

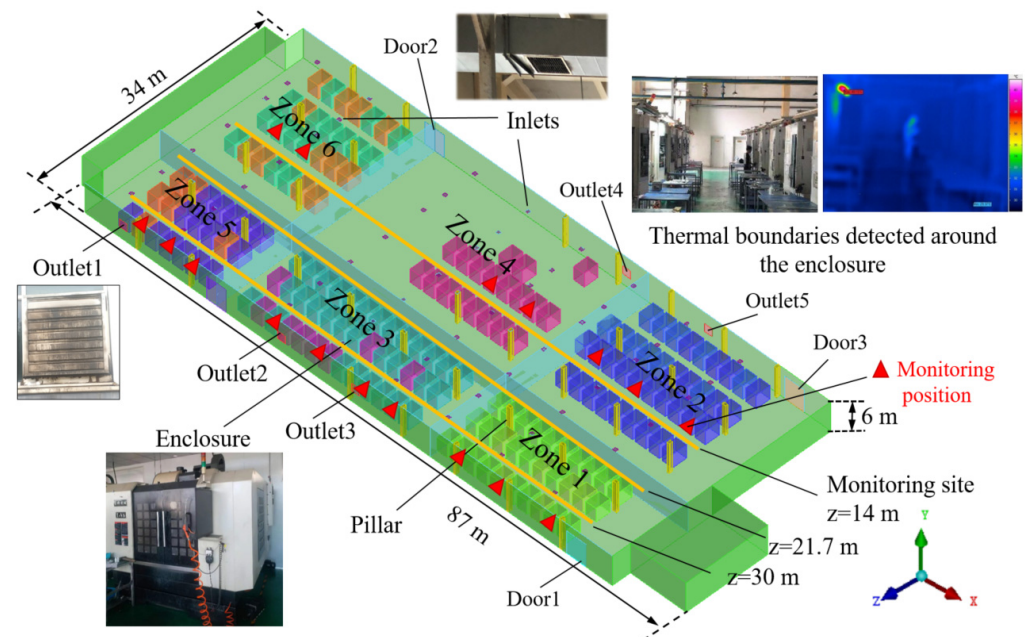


Figure 1. Model of CNC machining workshop.

The workshop adopts both mechanical ventilation and air conditioning systems to control indoor air quality. The air conditioning system applies direct evaporation, refrigeration, and heating, with a heat pump system providing both cooling and heating water. As seen in Figure 1, the conditioned air enters the rooms through the diffusers above the working area and 4.2 m above the floor. There are a total of 56 diffusers evenly distributed in the workshop, with a dimension of 0.44 m \times 0.46 m. Five grilles are installed on the sidewalls, with a dimension of 1.22 m \times 1.22 m. During the time of the experiment, other doors and windows remained closed.

2.1.2. Particle Size Measurement

The determination of the actual size distribution of oil mist is helpful in providing the CFD simulation with the proper setting of particle properties [30]. There are three main methods for the measurement of particle size distribution: microscopy, sieving, and light scattering. The light scattering method refers to the scattering phenomenon of a monochromatic light beam on an air sample. By measuring the energy distribution

(scattering angle) of the scattered light, the particle size distribution can be calculated. In this study, to clarify the size distribution of oil mist particles in the actual workshop, we applied Aerosol Spectrometer TSI DustTrak (0.001–150 mg/m³, accuracy: 0.001 mg/m³) to detect the particle size in the workshop. The DustTrak monitor is an optical instrument that uses a 90° light scattering technique in which the amount of scattered light is used to estimate the PM mass concentrations [31]. The logging intervals of DustTrak were set to 1 min. The default “Factory Cal” with a photometric of 1.00 was used. We set up seven monitoring heights in the vertical direction (0 m, 1 m, 1.5 m, 2 m, 3 m, 4 m, 5 m), and two monitoring points (NO.1, NO.2) at 1.5 m in the horizontal direction.

2.1.3. Particle Concentration Monitoring

In the CNC machining workshop of this study, wet cutting is the main processing mode for manufacture, which leads to a large number of fine oil mist particles in the working area of the factory. The in-situ experiment data can reflect the real pollution situation and be used in the selection of ventilation strategies.

We used integrated sensors (manufacturer: Ikair Inc. China) to monitor the machining workshop on site, as shown in the red rectangle in Figure 1. The parameters included oil mist concentration, relative humidity, temperature, velocity, mass fraction of particles in the air supply, and the emission intensity of particles. PM2.5 refers to particles with a diameter of fewer than 2.5 µm. When particles pass through the laser light, the scattering signal from the optical sensor is digitally processed and measured. The pulse amplitude of particles with a diameter of fewer than 2.5 µm is different; hence the corresponding particle number is determined. The mass concentration of particles is detected by a fitted curve with the particle number [32].

We chose three sampling lines, $z = 14.0$ m, $z = 21.7$ m, and $z = 30.0$ m in the measurement. Measuring points were evenly distributed in workers’ working areas. The sensors were mounted on the top of the enclosure. This height is the general breathing height of workers, about 1.5 m above the ground. The monitored data are uploaded to the cloud server through Wi-Fi every five minutes. The study was conducted from 1 January 2020 to 30 June 2020. The detailed instruments used in the measurement process are summarized in Table 1.

Table 1. Lists the instruments used in the experiment.

Measuring Equipment	Parameters	Range	Accuracy
Testo 405i Hot-wire anemometer	Velocity (m/s)	0–30	±0.015
Telaire 7001 HOBO Data logger	CO ₂ concentration (ppm)	0–10,000	±50
A4-CG Particulate sensor	CO ₂ concentration (ppm)	0–2500	±1
Vario CAM Infrared imager	Concentration of particle matters (µg/m ³)	0–6000	±10
	Surface temperature (°C)	0–100	±1.5
APS 3321	Particle size (µm)	0.5–20	±0.02 (1 µm), ±0.03 (10 µm)

2.1.4. Infiltration Rate of Enclosures

In the CNC machining workshop, each machining equipment was surrounded by an enclosure. The length, width, and height of the enclosure are 1.6 m, 1.28 m, and 2.09 m, respectively. The oil mist concentration and infiltration rate in the covered enclosure are important factors in determining the release rate of oil mists. We monitored the concentration of oil mist particles in the enclosure with the A4-CG particulate matter sensor (manufacturer: Yishan Inc., China) with the LoRa wireless module uploading data every 10 min, and its detailed information is given in Table 1. The real-time monitoring experiment of oil mist was conducted inside a typical enclosure of the CNC machining workshop. The experiment of monitoring was conducted from 3 January 2020 to 5 January 2020. In this period, this equipment had both a working stage and a standby stage. In order to obtain

the infiltration rate of the enclosures under two stages, we adopted carbon dioxide (CO_2) as a tracer gas and applied the decay method [11]. The initial CO_2 concentration in the enclosure increased up to 2500 ppm by controlling the flow regulator from the CO_2 tank. A mixing fan was activated simultaneously to distribute the CO_2 and mix it with the ambient air inside the enclosure. We adopted Telaire 7001 and HOBO data logger to monitor the CO_2 concentration, as seen in Table 1. It should be noticed that the worker might open the operation door frequently to check the machining progress; thus, a door state sensor was installed to record the frequency of door opening. According to the worker's operating frequency, the data were recorded every 10 min by the data loggers, as shown in Figure 2.

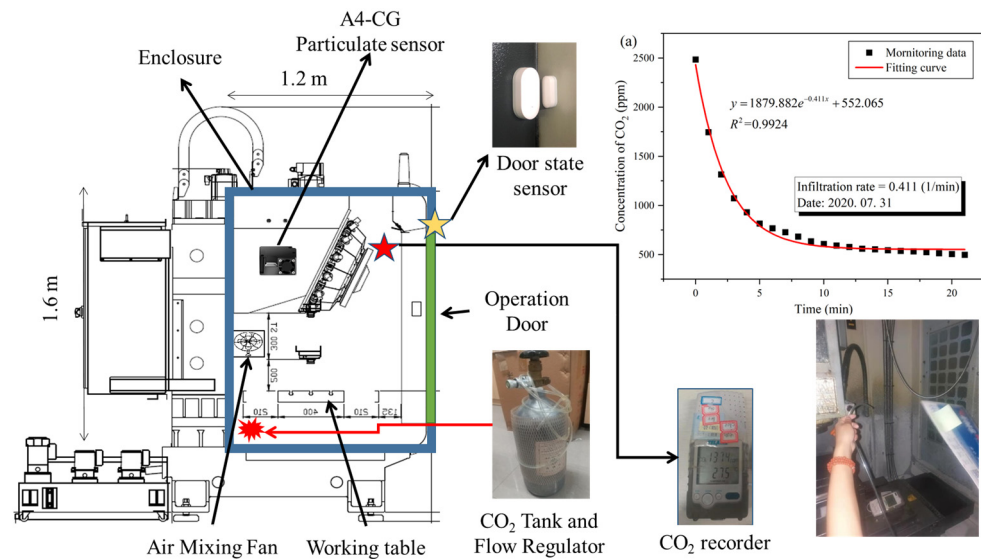


Figure 2. Measurement setup for infiltration rate in the enclosures, where tracer gas decay method with CO_2 was applied. A door state sensor was applied to record the state of the operation door. (a) Concentration of CO_2 and its fitting curve inside B2 enclosure.

The particle sensor was used to monitor the concentration of particles in the enclosure. The tracer gas decay method was used to measure the infiltration rate of the enclosure. Through these two values, the oil mist release rate can be obtained. The particle release rates were calculated according to the infiltration rate and the monitored particle concentration difference. By monitoring the particle concentrations inside and outside the enclosures, the release rate of particles from each enclosure $R(t)$, $\mu\text{g/s}$, was obtained by Equation (1).

$$R(t) = I(t) [C_i(t) - C_o(t)] \quad (1)$$

where, $I(t)$ is the infiltration rate of the enclosures, m^3/s ; $C_{i,p}(t)$ and $C_{o,p}(t)$ are the particle concentrations inside and outside the enclosures, $\mu\text{g}/\text{m}^3$. To calculate the release rate of particles from the enclosures $R(t)$, we measured $I(t)$, $C_i(t)$, and $C_o(t)$, in which $C_i(t)$ was measured at the center of the enclosure and $C_o(t)$ was measured in the working area at the aisle of the workshop.

The tracer gas decay method was applied to acquire the infiltration rate $I(t)$. The decay rate of CO_2 concentration can be applied to obtain the air exchange rates. In conditioning that the air infiltration rate through the enclosure is constant during the test, the change of CO_2 concentration inside the enclosure is calculated by Equation (2).

$$C_{i,c}(t) = P(0)e^{-Pt} \quad (2)$$

where P is the air change rate, $1/\text{s}$, in the enclosure within a certain time period t ; $V = 3.22 \text{ m}^3$ is the inner volume of enclosure, unit: m^3 ; $C_{i,c}(t)$ is the CO_2 concentration, unit: ppm. The

attenuation law of CO₂ follows a logarithm curve, and hence the value of P can be obtained by the logarithmic regression analysis method. Subsequently, $I(t)$ is obtained from Equation (3).

$$P(t) = \frac{I(t)}{V} \quad (3)$$

2.2. Numerical Simulation

2.2.1. Computational Domain

This study adopted CFD for solving the steady-state mass and momentum equation through a finite volume procedure in the numerical model, using the commercial solver ANSYS Fluent 19.0. The general form of the governing equations can be written as:

$$\frac{\partial(\rho\phi)}{\partial t} + \text{div}(\rho u\phi) = \text{div}(\Gamma \text{grad}\phi) + S \quad (4)$$

in which ϕ represents the general variables, Γ the effective diffusion coefficient, and S is the source term.

Due to the complicated geometry of the workshop indoor spaces, in this study, the unstructured grid is used for spatial discretization. To test the grid independence, a grid sensitivity analysis test was conducted. Considering the computational accuracy and cost, three grid numbers of 6,400,000 (Fine), 820,000 (Medium), and 340,000 (Coarse) are generated. In terms of medium mesh, the maximum grid size was 0.80 m, the minimum grid size was 0.01 m, and the grids close to diffusers and enclosures were locally encrypted. The medium mesh grid did not contain negative mesh volume. The orthogonal quality of the mesh was greater than 0.4, and the skewness was less than 0.90. The aspect ratio of the grid was less than 11.8, and a larger aspect ratio of the grid was allowed in the area without a strong lateral gradient (such as the interior of the boundary layer). The near wall grid was refined in order to use the standard wall function, which required that the average near wall y^+ value was within the range of 30–200. For the independence analysis, two representative lines were selected, one in the working area ($y = 1.5$ m) and another near the ceiling height ($y = 3.5$ m). The results of the grid independence test are depicted in Figure 3, reflecting good consistency between medium and fine meshes. However, it is considered that coarse mesh has poor wind speed fitting at $y = 3.5$ m in Figure 3b. Therefore, the medium mesh was finally selected for subsequent CFD study.

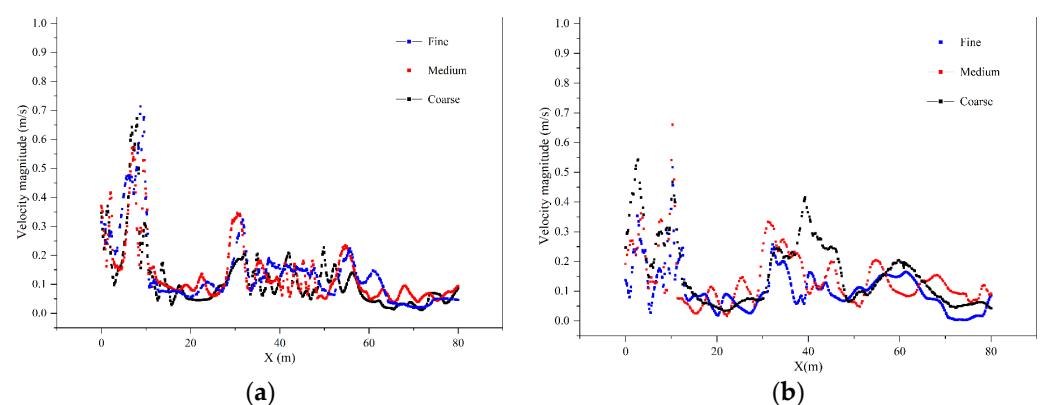


Figure 3. Grid independence analysis: (a) in the breathing height ($x = 14$ m, $y = 1.5$ m); (b) close to the enclosure ceiling ($x = 14$ m, $y = 3.5$ m).

2.2.2. Boundary Conditions

The boundary conditions for CFD simulation were measured from an in-situ experiment and detailed information on measuring equipment is shown in Table 2. The air supply angle was equal to the factory value of the jet angle of diffusers. The number of running machines at this time was observed automatically by the door state sensors. From the thermal measurement in the workshop, we noticed that there was little difference between

the temperature of the wall and the temperature of the equipment surface. Hence, it can be assumed that there is no obvious heat source in the machine workshop, and the energy equation is not opened. Adiabatic boundary conditions are assumed on the wall. This is because massive metal cutting fluids are applied in the machining process to reduce the heat released from the machining process.

Table 2. Measured boundary conditions applied for CFD validation for different zones in the CNC workshop.

Measuring Parameters	Boundary Conditions	Inputs
Air supply inlets	Air supply velocity (m/s)	3.21 ± 0.10
	Air supply angle (°)	45
	Air temperature(°C)	25
Particles from enclosures	Mass concentration ($\mu\text{g}/\text{m}^3$)	From A4-CG Particulate sensors
	The infiltration rate of fully enclosures (m^3/s)	From tracer gas experiment
	Zone 1	16
	Zone 2	11
Number of machines (on)	Zone 3	8
	Zone 4	0
	Zone 5	6
	Zone 6	6
	Thermal boundary	Enclosure Wall (°C)
	Meta-machining fluid (°C)	25
	Other inner walls (°C)	32

The boundary condition definitions of particle field concerned not only the turbulence effect on particle motion but also the deposition effect by rigid surfaces. When particles contact walls during movement, there are different movement behaviors in terms of rebound, capture, escape, and formation of wall liquid film. Zhang [33] found that setting a small rebound coefficient for the wall boundary condition can predict the particle concentration in the workshops. Hinds [34] found that particles did not have enough energy to rebound from a solid surface; therefore they were most often attached to the surface. Zhang and Chen [35] suggested that using a small restitution coefficient would be more reasonable than treating the particles as completely trapped, and the coefficient determined by Zhang and Chen was adopted in this study.

2.2.3. Numerical Setup

To ensure computational accuracy, the discretization scheme was set as a second-order upwind for all variables. The SIMPLE algorithm (Semi-Implicit Method for Pressure Linked Equations) [36] was applied to calculate the computation of pressure and velocity terms. Additionally, the renormalization group (RNG) $k-\varepsilon$ model was used to resolve the turbulence field due to its optimal performance justified in existing studies in terms of reasonable accuracy, computational cost, and robustness [37,38].

At present, the simulation of the particle field inside buildings can be either the Euler model or the Lagrange model. The Euler model treated the particulate matter as a gas without considering the deposition of particulate matter [33], while the Lagrangian model resolved the steady-state particle field by iterating the trajectories of discrete particles by solving the differential equation of particle force. We applied the Lagrangian model for this study because it obtained satisfactory prediction results for indoor particle, velocity, and temperature fields in similar buildings [39].

2.2.4. Model Validation

To validate the numerical model, the monitored particle concentration and velocity in the real machining workshop were used. Figure 1 shows the line distribution where the measuring points were located. The experimental instruments used in the measurement process are summarized in Table 1. The established grid files and boundary conditions

were imported into Fluent solver. The source of particles was monitored by particle sensors. In the CFD simulation, particles from enclosures with the operation door closed with mass concentration equaled $755 \mu\text{g}/\text{m}^3$, and the release rate from full enclosures was $6.545 \pm 0.047 \mu\text{g}/\text{s}$.

As shown in Figure 4, the predicted velocity of $z = 14.0 \text{ m}$, $z = 21.7 \text{ m}$, and $z = 30.0 \text{ m}$ are consistent with the measured values, with deviations less than 15%. Because of the complex site conditions, uncertainties in the field measurements, and approximations in the CFD simulation, a perfect agreement between the CFD results and the experimental data was not easy to achieve. Thus, we consider the differences to be acceptable and the CFD model to have been validated. The comparison with the experimental results has a similar simulation error of less than 15% in terms of the scale size laboratory study by Wei et al. [23] and the field measurement study by Zhang et al. [20]. The predicted particle concentration also agreed well with the measured values with deviations less than 10%. Thereby we applied the CFD model to analyze the particle transfer and velocity field in the following study.

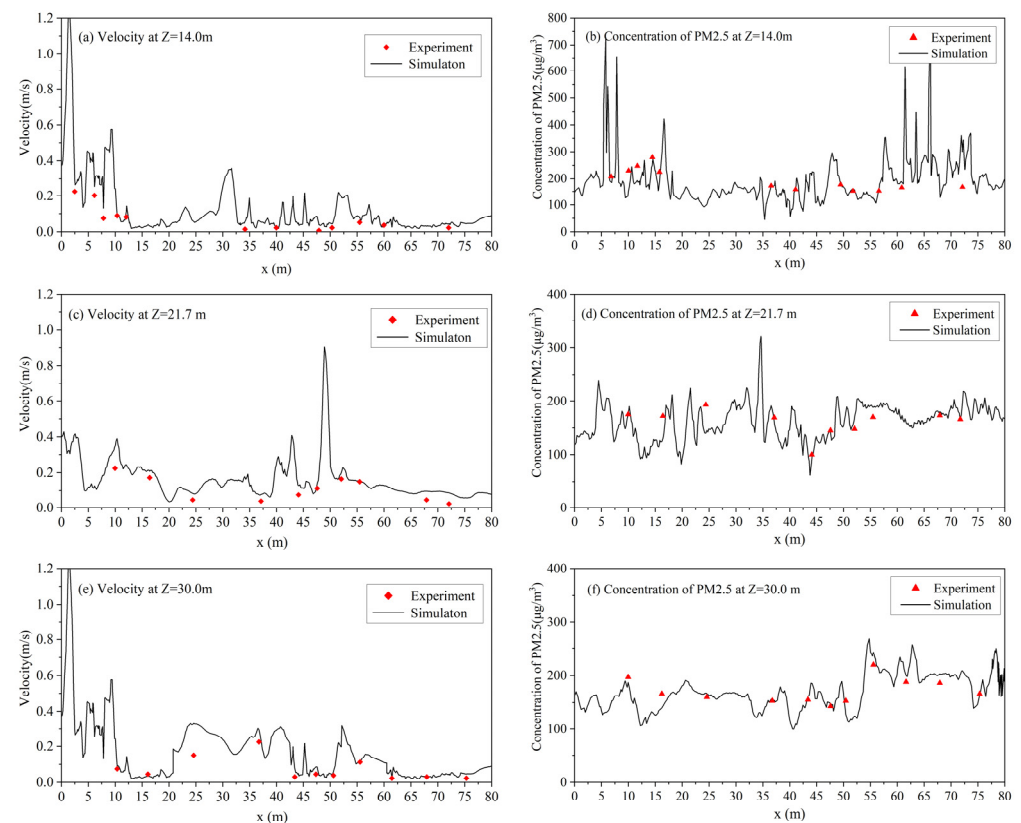


Figure 4. CFD validation of air velocity and concentration of particles in the working area of the workshop: (a,b) velocity and concentration of PM 2.5 at $z = 14.0 \text{ m}$; (c,d) velocity and concentration of PM 2.5 at $z = 21.7 \text{ m}$; (e,f) velocity and concentration of PM2.5 at $z = 30.0 \text{ m}$.

2.3. Ventilation Strategies

Figure 5 shows the layout of five ventilation strategies being investigated in this study. In general, the ventilation performance of four displacement ventilation strategies and a mixed ventilation strategy were compared in this study. Despite the arrangement of inlets and outlets, the physical model was almost the same among various strategies. According to our observations in the workshop, most of the machining work was done by the automatic, programmed equipment. Operators did not stand still in one place; instead, they walked randomly around the workshop; thus, we did not consider the influence of human activity on the airflow and particle field. In the displacement strategies, the

influence of the position of the inlets and outlets on the dispersion of particles and the airflow distribution was investigated.

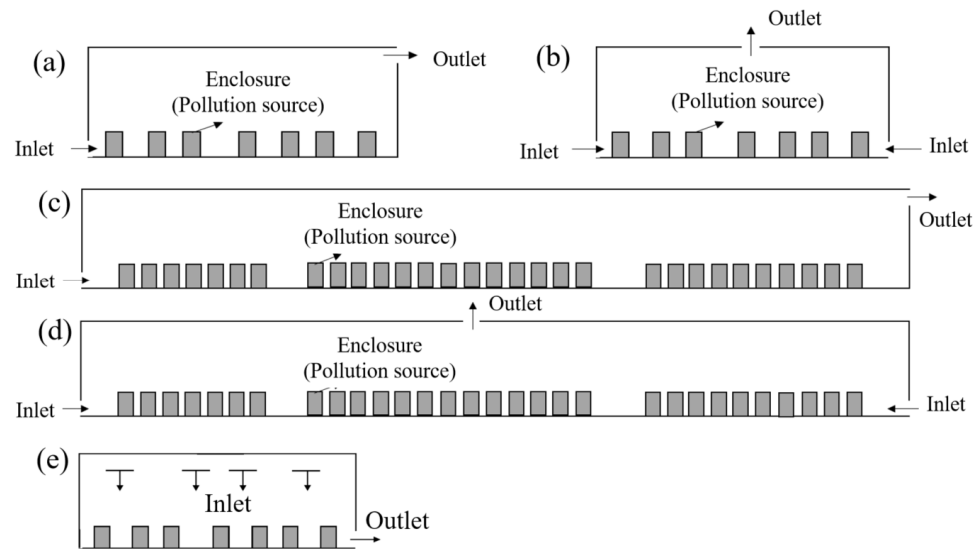


Figure 5. Schematic layout of various ventilation strategies, (a) single-side transverse ventilation, (b) bilateral transverse ventilation, (c) unilateral longitudinal ventilation, (d) bilateral longitudinal ventilation, (e) mixed ventilation.

Wang et al. [30] studied a machining factory about the particle size distribution and unit emission rate of oil mist. They found that the increase in air exchange rate had little influence on the concentration of oil mist in factory workshops, with only 0.05 h^{-1} needed to fulfill the standard limit of 0.5 mg/m^3 . In this study, the ventilation rate was the same among various ventilation strategies to compare the ventilation performance. The ventilation rate Q calculation is based on the mass balance of the particle inside and outside the buildings.

$$Q = \frac{M}{C_y - C_j} \quad (5)$$

where M is the total release rate of particles, $\mu\text{g/s}$, which was the sum of the release rate from enclosures; all machines in enclosures were activated for the comparisons. C_y is the maximum allowable concentration of indoor mass particle, mg/m^3 , which were 0.5 mg/m^3 as defined by NIOSH [10]. C_j is the concentration of pollutants entering the workshop room, mg/m^3 equaling the monitored particle matter sensors. Based on these settings, the yielded ventilation rate was $20,000 \text{ m}^3/\text{h}$.

The inlets and outlets' geometry sizes were defined according to the industrial building HVAC standards, encompassing the size of $3 \text{ m} \times 0.6 \text{ m}$ and $6 \text{ m} \times 0.6 \text{ m}$. According to China GB50019-2015 [40], for the ventilation of industrial buildings, the air supply speed was 0.25 m/s , which did not exceed 0.5 m/s [40]. Consequently, the inlet air speed was defined at 0.5 m/s . For the displacement ventilation system with inlets at one side, the size of the air supply inlet I_s is generally 0.1 times the maximum height of the workshop, which was equal to 0.6 m in this study. For displacement ventilation with inlets at two sides, the height of the air supply inlet I_s is generally 0.05 times the maximum height, which equals 0.3 m .

3. Results

3.1. Monitored Results

3.1.1. Particle Size Distribution

According to the experiment setup, we monitored the particle size of oil mist pollution in the vertical direction of the working area inside the workshop, and the test results are shown in Figure 6a. At the same time, in order to further represent the particle size of oil

pollution particles at the breathing height of workers ($y = 1.5\text{m}$), we drew the cumulative particle size distribution of particles, as shown in Figure 6b.

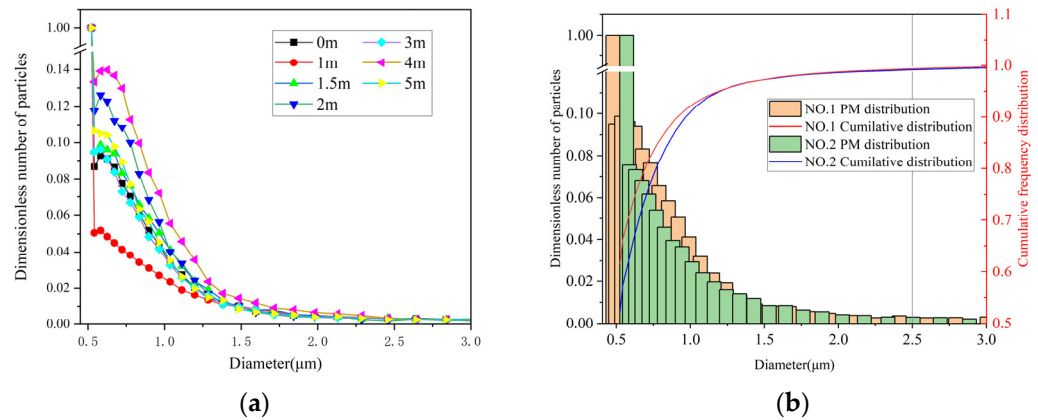


Figure 6. Size distributions of particles measured inside and outside the enclosure in the CNC workshop based on APS 3321: (a) particle size distribution at seven heights, (b) Dimensionless particles, and cumulative frequency distribution of particle size at 1.5 m.

We find that the particle size distribution in the CNC workshop differs at different heights. Among them, the dimensionless number of fine particles at 1 m is the lowest and the highest at 4 m. The reason why the particle size varied slightly at different heights may be because the water content in the particle rapidly evaporated after being emitted from the sources. A similar finding can be seen in previous research related to the particles containing water [41]. Nevertheless, the particle size is mainly within 0.5–1 μm. Similar results are shown in Figure 6b. About 99% of the particles are less than 2.5 μm in size, which indicates that the oil particles in the target plant studied in this paper are mainly PM 2.5.

3.1.2. Oil Mist Concentration in CNC Machining Workshop

Figure 7 presents the oil mist concentration over time in the different working areas of the workshop. The working area inside the workshop is divided into six zones. As seen in Figure 7, the mass concentration of oil mist between different zones has good followability. It may be ascribed to that the oil mist in each area is adequately mixed in the workshop. Therefore, when analyzing the concentration of oil mist in the workshop, the average concentration of the workshop can be used. It can also be seen that the concentration of oil mist in Zone 4 and Zone 5 is significantly lower than in other zones. This was because in two zones, the machining was conducted fewer times than in other zones, as seen in Table 1. In addition, the peak value of oil mist concentration in the workshop decreased gradually from winter to summer because the machining activities were reduced. Most importantly, the concentration of oil mist in the workshop exceeded the NIOSH standard. Therefore, it was necessary to improve the ventilation mode because it could not completely eliminate the oil mist produced in the workshop.

3.1.3. Infiltration Rate of Enclosures

Table 3 shows the measurement results of the infiltration rate by the tracer gas decay method. The absolute value of the coefficient of the fitted curve is the value of the air change rate, P . The R^2 of the equations is greater than 0.96, indicating that the regression curve had a good quality of fit with the monitoring data.

The infiltration rate of the enclosure where the spindle was stationary was equal to $1.274 \pm 0.440 \text{ m}^3/\text{s}$, as seen in enclosure B1–B7, while in the dynamical condition in C1, the value was $1.117 \pm 0.208 \text{ m}^3/\text{s}$. Thus, the machine movement had some influence on the infiltration rate. It was mainly because internal mechanical movement drives the air motion. When the moving air collides with the enclosure, the moving air converts its

dynamic pressure into static pressure, increasing the air pressure inside the enclosure. In order to analyze the influence of the rotation speed, travel, and moving speed of the vertical spindle on the infiltration rate, an experiment was carried out in a single enclosure, and the experimental results are shown in Table 3. According to the experiment results, the moving speed of the spindle has an obvious effect on the infiltration rate of the enclosure, and its sensitivity was superior to the rotation speed and travel distance. In this CFD study, the infiltration rate was set as $1.117 \text{ m}^3/\text{s}$ in order to determine the release rate of oil mist during the machining process.

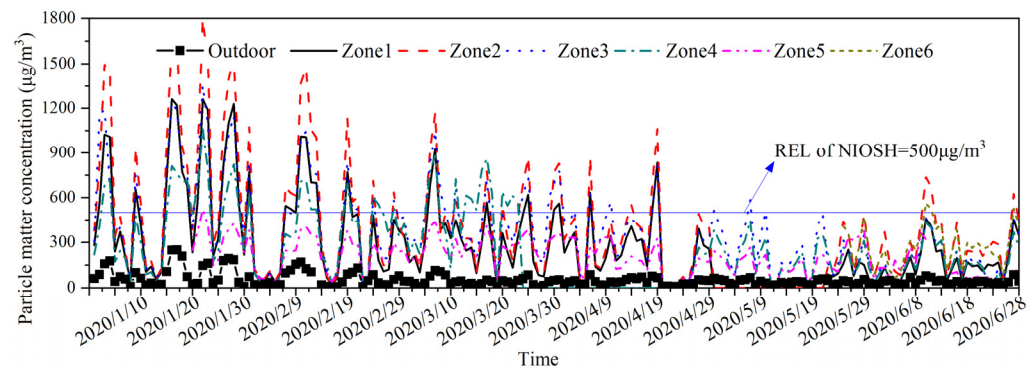


Figure 7. Long-term monitored particle matter concentration inside and outside the CNC machining workshop. Zones 1–6 were the division of the working area in the workshop.

Table 3. Results of tracer gas experiment by CO_2 under different working scenarios in workshop enclosures.

Enclosure Number	Rotation Speed of Spindle (1/min)	Travel Distance of Spindle (min)	Moving Speed of Spindle (mm/min)	Infiltration Rate (m^3/s)
B1	0	0	0	1.472
B2	0	0	0	1.448
B4	0	0	0	1.523
B5	0	0	0	1.739
B6	0	0	0	0.603
B7	0	0	0	0.861
C1	2000	200	1000	1.307
	2000	200	3000	0.758
	5000	100	1000	0.959
	5000	200	2000	0.980
	5000	200	3000	0.883
	5000	300	1000	1.204
	5000	300	3000	1.338
	8000	100	2000	1.078
	8000	200	1000	1.255
	8000	200	3000	1.106
	8000	300	2000	1.418

3.1.4. Oil Mist Concentration Inside the Enclosures

To effectively control the concentration of oil mist in the workshop and analyze the strong source of pollutants in the workshop, we conducted monitoring inside and outside the enclosure in the machining workshop. The monitoring results of 5 January and 28 June 2020 were analyzed as an example, as shown in Figure 8a,b. The machining equipment inside the enclosures was activated in these two days. The particulate matter concentration inside the enclosures was monitored.

As shown in Figure 8a, the machine began to process parts at 8:00 a.m., and the concentration of oil mist inside the enclosure began to surge. During the operation of the machine, the concentration of particulate matter fluctuated around $1400 \mu\text{g}/\text{m}^3$. During lunchtime, from 11:00 to 11:30 a.m., the machine stopped running, and the concentration

of particulate matter inside the enclosure dropped to $800 \mu\text{g}/\text{m}^3$. When the machine ran from 11:30 to 17:30, the concentration of particulate matter in the enclosure reached $14,300 \mu\text{g}/\text{m}^3$; From 17:30 to 18:10, the machine stopped running, and the concentration of particulate matter inside the enclosure dropped to $1000 \mu\text{g}/\text{m}^3$. From 18:10 to 19:30, when the machine was running, the concentration of particulate matter in the enclosure first increased and then fluctuated around $1600 \mu\text{g}/\text{m}^3$. The machine was shut down at 19:30, and the concentration of particulate matter inside the enclosure remained at $1000 \mu\text{g}/\text{m}^3$. When the equipment inside the enclosure was running, due to the use of cutting fluid, the concentration of particles in the enclosure fluctuated at $1400 \mu\text{g}/\text{m}^3$. When the equipment stopped running, the concentration of particulate matter in the enclosure decreased by at least $600 \mu\text{g}/\text{m}^3$. A similar finding can be observed in another enclosure in the workshop, as seen in Figure 8b. Due to the shorter working time, the average concentration of particulate matter in the enclosure was close to $600 \mu\text{g}/\text{m}^3$ lower. It demonstrates that the operation of equipment significantly impacts the concentration of particulate matter outside the enclosure in the workshop.

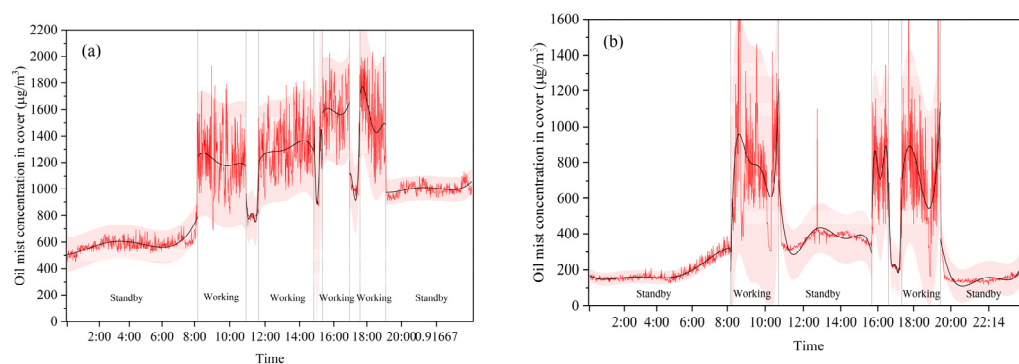


Figure 8. The measured oil mist concentration in two enclosures on 3rd January 2020.

3.2. Ventilation Strategies

3.2.1. Particle Concentration Distribution

The distribution of particle concentration in the working section is shown in Figure 9. The particle concentration in some regions of the working area under single-side transverse ventilation, bilateral transverse ventilation, and unilateral longitudinal ventilation exceed the expected value of $0.5 \text{ mg}/\text{m}^3$. However, the area exceeding the standard is different among different ventilation strategies. The single-side transverse ventilation in Figure 9a and unilateral longitudinal ventilation in Figure 9c exceed $0.5 \text{ mg}/\text{m}^3$ in more areas than the bilateral transverse ventilation and bilateral longitudinal ventilation. This happened because strong convective airflow was generated in the building's width and length direction, respectively, in bilateral transverse and bilateral longitudinal ventilation. The fresh airflow sent through the air supply inlet can thus penetrate the entire workshop space to dilute the particle concentration in the working area. It is, thus, highly recommended to apply bilateral side wall inlets in such buildings.

The high concentration area under bilateral transverse ventilation is smaller than that of bilateral longitudinal ventilation. Under bilateral longitudinal ventilation, it is concentrated in the working area; on the contrary, in the non-working area under bilateral transverse ventilation. This is because the airflow from the transverse sides has to pass through the gap between the enclosures in the workshop when the gap size is almost the same. Even though the flows can be almost evenly distributed in each gap to remove the pollutants between the operator's work area and the enclosures, the flow resistance is still high because multiple objects are located between the gaps. Because the width of the operators' working area in the width direction is much larger than the gap between the enclosures, the airflow can pass through the working area with less resistance under longitudinal ventilation. Therefore, the particle concentration in the working area is lower than in bilateral transverse ventilation.

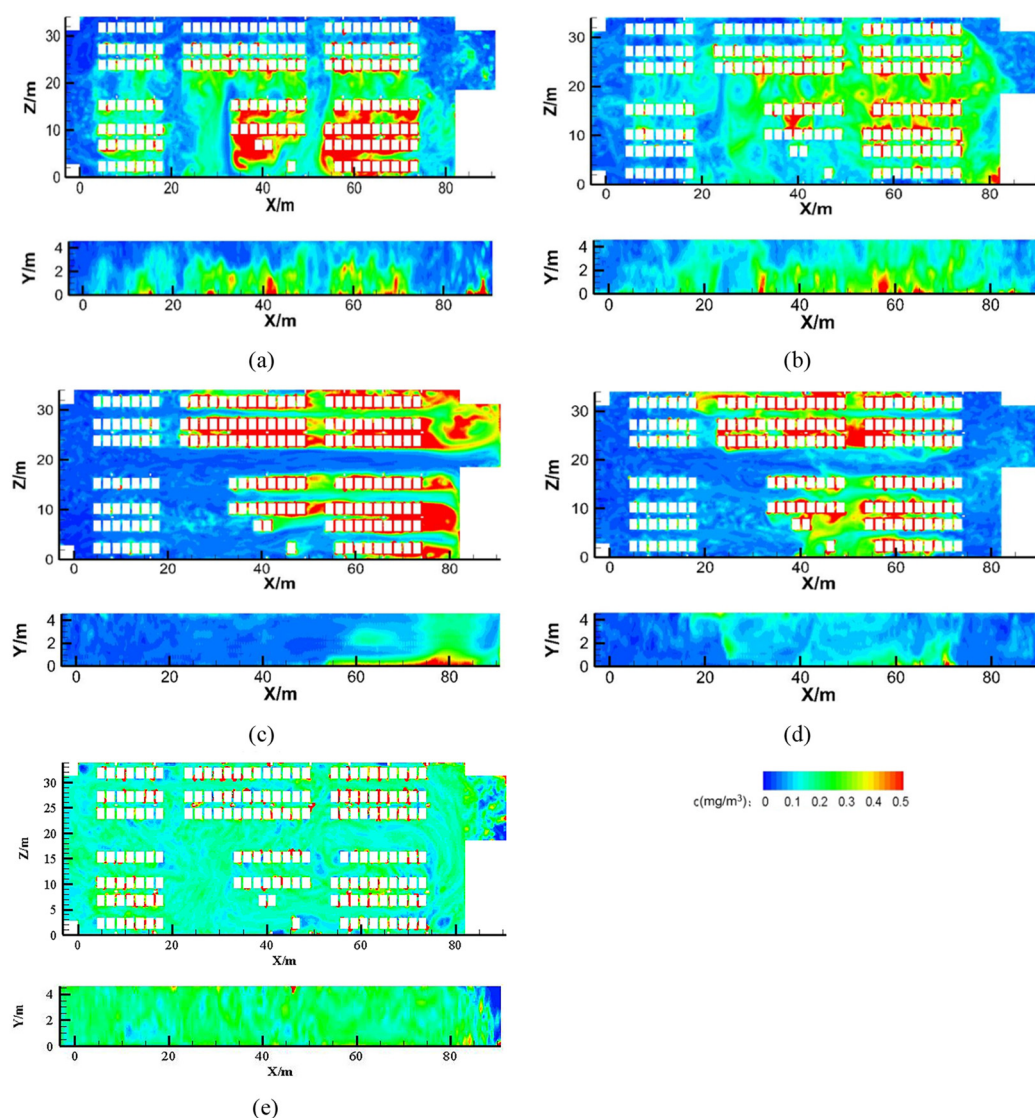


Figure 9. Particle concentration distribution at the horizontal and vertical section planes, (a) single-side transverse ventilation, (b) bilateral transverse ventilation, (c) unilateral longitudinal ventilation, (d) bilateral longitudinal ventilation, (e) mixing ventilation.

Figure 9e shows that under mixed ventilation, the distribution of particle fields in the longitudinal and transverse directions is very uniform, but the concentration value is high. Under mixed ventilation, the particle concentration in the working area is diluted by complete mixing to make it meet the standard requirements. Some studies show that the mixing ventilation is not conducive to the discharge of particulate matter in the workshop, especially in large-space industrial buildings, because of the subsequent high increase in ventilation rates and energy consumption. In addition, the mixed ventilation system contains components such as ventilation ducts and multiple diffuser inlets, which largely increase the construction cost.

3.2.2. Airflow Patterns

Figure 10 exhibits the airflow patterns in the working area under various ventilation strategies. In order to more clearly show the airflow organization of each zone in the room, we show the position and shape of the big vortex in the figure. Because of the single-side unilateral ventilation, the airflow from the air inlet cross through the whole cross-section and is discharged from the air outlet; it is evident that there is a large eddy current on the longitudinal section, as seen in Figure 10a. The large eddy is broken into many small-size

vortices by enclosures. These eddies and vortices on the longitudinal section cause particles to gather in this area and form a high-pollution area. The bilateral transverse ventilation presents a low concentration of particles because the incoming air from inlets travels at a shorter distance than the single-side unilateral ventilation before approaching the middle area, as seen in Figure 10b. There is almost no vortex, and the airflow patterns were very similar for unilateral and bilateral longitudinal ventilation, as seen in Figure 10c. Some vortexes exist downwind of several enclosures under the longitudinal ventilation, creating highly concentrated zones of particles in these areas in Figure 10c. In mixed ventilation, the airflow patterns were very uniform so that the particles released from the pollution sources were thoroughly mixed, as seen in Figure 10e.

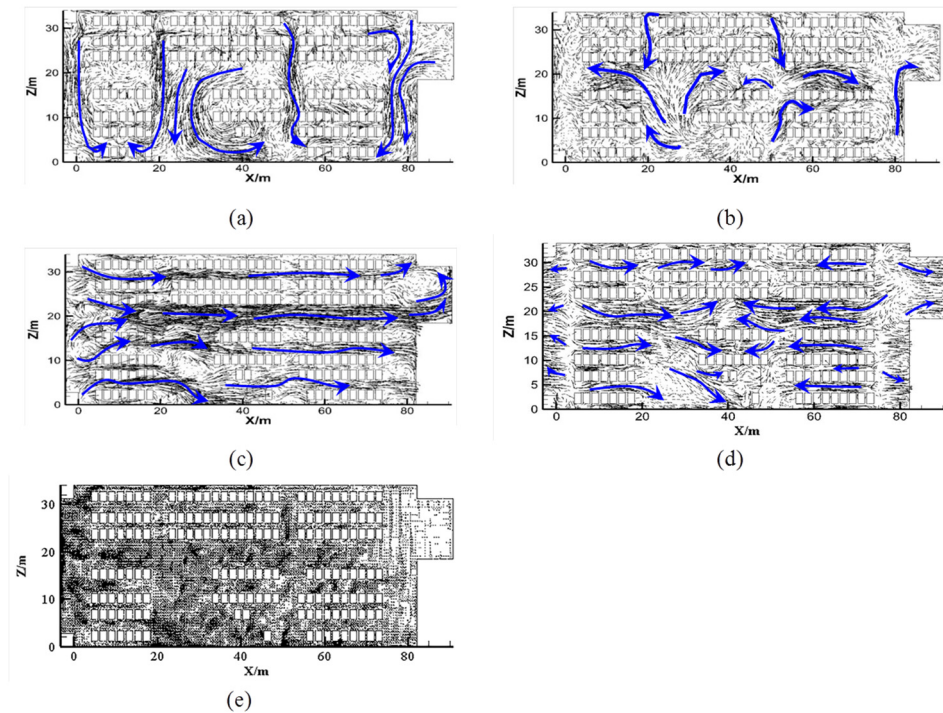


Figure 10. Airflow patterns at the horizontal section plane $y = 1.5$ m, (a) single-side transverse ventilation, (b) bilateral transverse ventilation, (c) unilateral longitudinal ventilation, (d) bilateral longitudinal ventilation, (e) mixing ventilation.

3.2.3. Improved Ventilation Strategies

In this study, the ventilation strategies were optimized according to the following evaluation indexes.

- (1) Average particle mass concentration in the working area at respiratory height was calculated as an evaluation index. In this study, the simulated particle size was $2.5 \mu\text{m}$. The mass concentration in the working area was averaged for the comparisons.
- (2) Mean age of air is an index used to investigate the time when the air at a certain point or the whole space is renewed. A user-defined arbitrary scalar Φ_i represented the mean age of air in the commercial solver. The transport of scalar was solved by one additional convection-diffusion equation:

$$\frac{\partial \rho \Phi_i}{\partial t} - \nabla (\Gamma_i \nabla \Phi_i) = S_{\Phi_i}, \quad (6)$$

$$\Gamma_i = 2.88 \times 10^{-5} \rho + \frac{\mu_{eff}}{0.7}, \quad (7)$$

where t is time (s), ρ the fluid density (kg/m^3), ϕ_i is the scalar to be solved, v is the fluid velocity (m/s), Γ_i is the diffusion coefficient of the scalar, and S_{ϕ_i} is the source term of the scalar, μ_{eff} is the effective viscosity of the air.

- (3) Ventilation efficiency is an index used to investigate the energy utilization effectiveness of a certain air distribution form. The higher the ventilation efficiency indicates, the better the system's performance. The theoretical calculation formula of ventilation efficiency, E_T , is calculated by Equation (6).

$$E_T = \frac{C_e - C_s}{C_b - C_s}, \quad (8)$$

where C_e is the average particle concentration at outlets, $\mu\text{g}/\text{m}^3$; C_b is the average particle concentration at respiratory height, $\mu\text{g}/\text{m}^3$; C_s is the average particle concentration at air supply inlet, $\mu\text{g}/\text{m}^3$, which equals zero in this study.

In the above five ventilation strategies, considering a safe and healthy operating environment, bilateral longitudinal ventilation can better control the concentration of particulate matter in workers' breathing areas. Additionally, the ventilation efficiency is higher than other ventilation strategies. The bilateral longitudinal ventilation had low air freshness in the middle area of the workshop, making the concentration of particulate matter in Zone 3 and Zone 4 exceed the standard. To solve this problem, eighteen spoiler fans are designated in the middle area of the workshop. In the CFD simulation, the axial fans were set as internal fans; the pressure drop value adopts a constant value of 100 Pa, and the installation height is 0.5 m above the floor. The boundary conditions of the wall and the return outlet are the same as other ventilation strategies, and the axial fans are set as the internal fan in the simulation. The layout of the axial fans is shown in Figure 11.

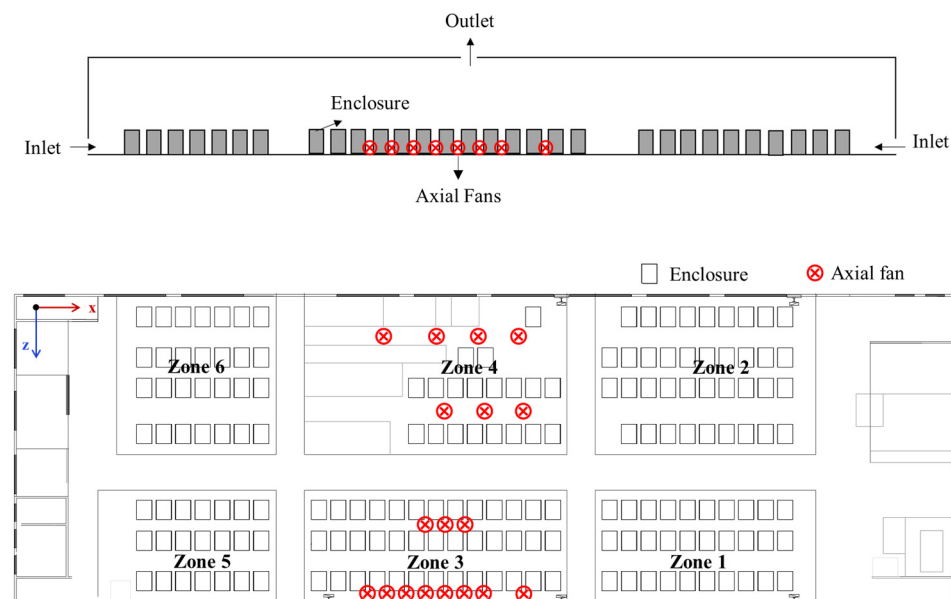


Figure 11. Layout of improved bilateral longitudinal ventilation by placing axial circulation fans in the center of the workshop, where \otimes represent the location of axial fans. The air outlet direction of the fans is vertically upward to the ceiling outlet of the workshop.

The different ventilation strategies were comprehensively compared in the horizontal plane ($y = 1.5$ m) and the vertical sections by the averaged values of evaluation indexes ($z = 14.0$ m, $z = 21.7$ m, and $z = 30.0$ m), as seen in Figure 11. The bilateral longitudinal ventilation best controls the particle concentration in the operators' working area. The bilateral transverse ventilation had the lowest mean age of air and thus achieved the best ability to deliver fresh air in the working area. In addition, the ventilation efficiency of unilateral longitudinal ventilation is higher than that of other ventilation strategies. It is

conclusive that bilateral longitudinal ventilation and mixing ventilation are superior to other strategies in terms of ventilation efficiencies and particle concentration.

At the same time, the simulation result of adding spoiler fans is shown in Figure 12. It can be seen that in each section increases, after the addition of spoiler fans, the air age of all sections in the workshop decreases significantly, the concentration of particulate matter at respiratory height decreases, and the ventilation efficiency in the whole workshop increases. Therefore, the addition of a spoiler fan will reduce thermal comfort. Moreover, it is very favorable for removing particulate matter and air freshness.

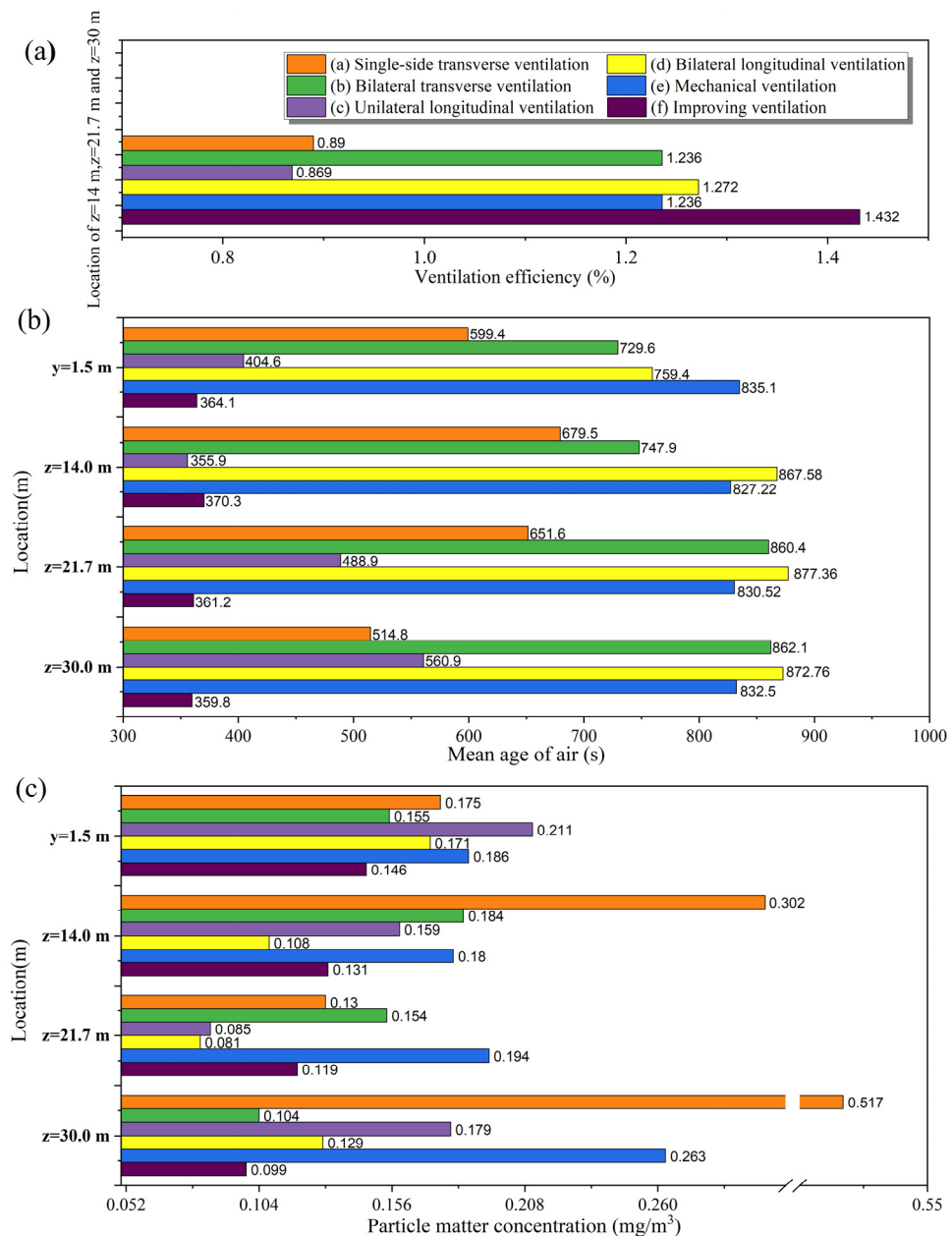


Figure 12. Comparisons of various indoor air evaluation indexes in different ventilation strategies (a–c).

4. Discussion

4.1. Ventilation Strategies in Workshop

With the same ventilation rate, the location of air supply inlets and outlets directly affects the ventilation efficiency of displacement ventilation. When the ventilation rates are too large, it causes an obvious human draft sensation to the operators in the CNC machining workshop. Furthermore, some regions in the workshop may be overheated.

When the ventilation rate is low, it cannot completely remove pollutants from the room and affect the health of operators. However, Wang et al. found from in-situ measurements that ventilation rates had small effects on the mass concentration of oil mist particles in machining workshops, especially for particle sizes below 5 μm [30]. Their results also show the quantity concentration does not seem to correlate with the ventilation rates. Jia et al. investigated the influence of ventilation rate on the performance of displacement ventilation strategy in another machining workshop [42]. It shows the varied ventilation rates achieved different concentration distributions of particulate matter in the workshop. Chen and Zhao found that the ventilation rate greatly influenced the distribution of particles with varying particle sizes in the displacement ventilation strategy [43]. The ventilation rate had a small effect on the removal efficiency of small-sized particles but had an enormous impact on the particle distribution in the workshop.

The design of airflow patterns is to supply sufficient air to a local working area or contaminated area in large machining workshops. By comparing five ventilation strategies in this study, it is interesting to see that the displacement ventilation strategy had better performance than the mixing ventilation in terms of ventilation efficiency. The workshop corridor in displacement ventilation can be used as a fresh air channel to achieve high ventilation efficiency in the working area. Due to the potential effect caused by thermal plumes from machining equipment, the indoor airflow may arise towards the ceiling outlet and carries away the polluted air. Wang et al. simulate a displacement ventilation system in a machining workshop with multiple heat resources. Displacement ventilation shows high removal efficiency of air pollutants in the breathing area [28]. Raimo et al. measured particle concentration and air temperature in the workshop, where displacement ventilation caused the stratification effect of the temperature field and particle field [22]. Even though the strength of indoor heat resources is weak, this study shows that displacement ventilation, especially bilateral longitudinal ventilation, can achieve better ventilation performance in CNC machining workshops. Moreover, bilateral longitudinal ventilation is superior to the mixing ventilation system by reducing the expenses of installing air ducts and air diffuser inlets [44].

Because the CNC machining workshop is a large space, air conditioning energy-saving measures are necessary to make healthy working environments. We also noticed that the inlet air could not pass through the entire workshop before reaching the work area. Instead, the inlet air gets only about half of this distance before being contaminated by the pollutants from enclosures. For transverse ventilation, the airflow flows from the upper and lower regions to the central zone of the workshop as a whole. When approaching the central zone of the workshop, the airflow begins to flow to the left and right sides. Because there is no air outlet on the left and right sides, the airflow cannot be eliminated in time but forms a vortex and then causes a dead ventilation zone. Hence, even though the uniformity is poor, the design of bilateral longitudinal ventilation avoids the airflow passing through the polluted area for a long time and can maintain ventilation efficiency in the working area. Bilateral longitudinal ventilation is the optimal solution of the four displacement ventilation strategies in terms of ventilation efficiency, only slightly higher than the other strategies in terms of mean age of air. The improvement of the age of air can be achieved by axial fans in the central zones of the CNC workshop.

4.2. Limitation of this Study

There are several limitations to this investigation. First, the research did not consider the temperature gradient and high humidity phenomenon in CNC machining workshops. The effect of humidity may influence thermal comfort but is not considered in the study. Second, since the current research assume the indoor space is well sealed, the air enters the workshop entirely from inlets and leaves the workshop through outlets. This would be valid only if enhanced sealing technologies were applied nowadays in industrial buildings. Nevertheless, natural ventilation might affect indoor airflow and contaminant distribution in scenarios where large openings exist, revolving doors, and open windows. Third,

the current research assumes a constant temperature at the solid inner walls in summer conditions; even though the thermal boundary was obtained through measurement from an actual CNC machining workshop, the seasonal variation of wall temperatures may affect indoor thermal conditions. Fourth, the application of other air conditioning systems, such as passive-chilled-beam systems, may affect the indoor airflow patterns and concentration field [45]. Fifth, a lot of results in this study were obtained from CFD simulation. Even though the CFD model captured the airflow and particle transmission with reasonable accuracy, further development of the CFD model should be continued in future studies.

5. Conclusions

The present study investigated the ventilation performance of five ventilation strategies in the CNC machining workshop. The physical model acquired the boundary conditions based on in-situ monitoring. The numerical models were used to simulate the distribution of mean age of air, particle concentration, and ventilation efficiency. The simulation results were validated based on the field-measured results. Consequently, the following conclusions are drawn:

- (1) The measurement results show that in the CNC workshop, the 99% cumulative mass concentration of particles was distributed within 2.5 μm , and the particle size distribution of particles at different heights in the workshop varied slightly. The infiltration rate of the fully closed enclosure was $1.117 \pm 0.208 \text{ m}^3/\text{s}$. The release rate of particles from the full enclosure was $6.545 \pm 0.047 \mu\text{g}/\text{s}$. The heat released from the enclosures can be neglected because the metalworking fluids take away most of the exclusive heat from the machining process.
- (2) This paper uses the RNG $k\text{-}\varepsilon$ model and the Lagrange method to simulate the workshop's velocity and particle field. The simulation results are consistent with the measured data in terms of velocity and particle mass concentration.
- (3) By comparing the simulation results of the five ventilation strategies with the same ventilation rates, the bilateral longitudinal ventilation strategy is superior to other methods in terms of average particle concentration and ventilation efficiency in the working area; Bilateral longitudinal ventilation strategy is only slightly higher than different strategies in terms of the age of air.
- (4) Bilateral longitudinal ventilation can make full use of the workshop corridor as the ventilation pathway. It can be further optimized by adding axial fans in the center of the workshop.

Author Contributions: Conceptualization, S.Q. and X.S.; Data curation, X.S.; Formal analysis, S.Q. and X.S.; Funding acquisition, X.S.; Investigation, X.S.; Methodology, S.Q. and X.S.; Project administration, X.S.; Resources, X.S.; Software, X.S.; Supervision, S.W., Z.L., W.W. and X.S.; Validation, S.Q., Y.L., A.L. and X.S.; Visualization, X.S.; Writing—original draft, H.Y. and X.S.; Writing—review & editing, H.Y. and X.S. All authors have read and agreed to the published version of the manuscript.

Funding: This study was conducted with the support of the Tianjin Key Laboratory of Indoor Air Environmental Quality Control. This work was supported by the National Science Foundation of China [Grant No.51878442]; This work was also supported by the National Nature Science Foundation of Tianjin [grant No. 19JCQNJC07100].

Institutional Review Board Statement: Not applicable.

Data Availability Statement: Not applicable.

Acknowledgments: This study was conducted with the support of the Tianjin Key Laboratory of Indoor Air Environmental Quality Control. This work was supported by the National Science Foundation of China [Grant No.51878442] and [Grant No. 19JCQNJC07100].

Conflicts of Interest: The authors declare that they have no known competing financial interests or personal relationships that could appear to influence the work reported in this paper.

Abbreviations

CNC	Computer Numerical Control
CFD	Computational Fluid Dynamics
RNG	Renormalization group
Nomenclature	
R	Release rate of particles from the enclosure, $\mu\text{g/s}$
I	Infiltration rate of the enclosure, m^3/s
P	Air change rate, $1/\text{s}$
t	Time, s
V	Inner volume of enclosure, $V = \text{constant} = 3.22 \text{ m}^3$
Q	Ventilation rate, m^3/s
M	Total release rate of particles, $\mu\text{g/s}$
$C_{i,p}$	Concentrations of particle matter inside the enclosure, $\mu\text{g}/\text{m}^3$
$C_{o,p}$	Concentrations of particle matter outside the enclosure, $\mu\text{g}/\text{m}^3$
$C_{i,c}$	Concentrations of CO_2 inside the enclosure, ppm
C_y	Maximum allowable concentration of indoor particle matter, mg/m^3
C_j	Concentration of pollutants entering the workshop room, mg/m^3
ρ	Fluid density, kg m^{-3}
v	Fluid velocity, m/s
μ_{eff}	Effective viscosity of the air, Pa s
Γ_i	Diffusion coefficient, m^2/s
E_T	Ventilation efficiency
C_e	Average particle concentration at outlets, $\mu\text{g}/\text{m}^3$
C_b	Average particle concentration at respiratory height, $\mu\text{g}/\text{m}^3$
C_s	Average particle concentration at air supply inlet, $\mu\text{g}/\text{m}^3$

References

- Guo, Y.; Sun, Y.; Wu, K. Research and development of monitoring system and data monitoring system and data acquisition of CNC machine tool in intelligent manufacturing. *Int. J. Adv. Robot. Syst.* **2020**, *17*. [[CrossRef](#)]
- Li, Q.; Wang, F.; Huang, C.; Yao, Z.; Xue, W. Study on Emission Characteristics and Influencing Factors of Oil Mist in Machining. *Lubr. Eng.* **2021**, *46*, 55–60.
- Graud, E.; Faisant, N. Occupational risk assessment of metalworking employees: The case of metalworking fluids. *Arch. Mal. Prof. L'Environ.* **2012**, *73*, 903–905.
- Eisen, E.A.; Smith, T.J.; Kriebel, D.; Woskie, S.R.; Myers, D.J.; Kennedy, S.M.; Shalat, S.; Monson, R.R. Respiratory health of automobile workers and exposures to metal-working fluid aerosols: Lung spirometry. *Am. J. Ind. Med.* **2001**, *39*, 443–453. [[CrossRef](#)]
- Lacasse, Y.; Girard, M.; Cormier, Y.J.C. Recent Advances in Hypersensitivity Pneumonitis. *Chest* **2012**, *142*, 208. [[CrossRef](#)]
- Mirer, F.E. New Evidence on the Health Hazards and Control of Metalworking Fluids Since Completion of the OSHA Advisory Committee Report. *Am. J. Ind. Med.* **2010**, *53*, 792–801. [[CrossRef](#)]
- Rim, K.-T.; Lim, C.-H. Biologically Hazardous Agents at Work and Efforts to Protect Workers' Health: A Review of Recent Reports. *Saf. Health Work.* **2014**, *5*, 43–52. [[CrossRef](#)]
- Weziak-Białowolska, D.; Białowolski, P.; McNeely, E. Worker's well-being. Evidence from the apparel industry in Mexico. Intelligent Buildings International. *Intell. Build. Int.* **2019**, *11*, 158–177.
- Hanson, R.; Ward, D.; Edmonds, J.; Escatell, J. *National Occupational Exposure Survey (NOES)*; National Institute for Occupational Safety and Health (NIOSH): Cincinnati, OH, USA, 1983; pp. 1–272.
- The National Institute for Occupational Safety and Health. *Criteria for a Recommended Standard: Occupational Exposure to Metal-Working Fluids*; NIOSH: Cincinnati, OH, USA, 1998; pp. 98–102.
- Tohti, E. *Industrial Ventilation Design Guidebook*; Goodfellow, H., Tahti, E., Eds.; Academic Press: Cambridge, MA, USA, 2001.
- Jurelionis, A.; Gagytė, L.; Prasauskas, T.; Čiužas, D.; Krugly, E.; Šeduikytė, L.; Martuzevičius, D. The impact of the air distribution method in ventilated rooms on the aerosol particle dispersion and removal: The experimental approach. *Energy Build.* **2015**, *86*, 305–313. [[CrossRef](#)]
- Meng, X.; Wang, Y.; Xing, X.; Xu, Y. Experimental study on the performance of hybrid buoyancy-driven natural ventilation with a mechanical exhaust system in an industrial building. *Energy Build.* **2020**, *208*, 109674. [[CrossRef](#)]
- Shi, X.Z.; Gao, N.P.; Zhu, T. Research on Concentration Distribution and Transmission Characteristics of Indoor Aerosol Particle—Influence to Human Particle Exposure. *Build. Sci.* **2009**, *25*.

15. Szczepanik-Ścisło, N.; Ścisło, Ł. Air leakage modelling and its influence on the air quality inside a garage. In Proceedings of the E3S Web of Conferences, Polanica-Zdrój, Poland, 16–18 April 2018; EDP Sciences: Les Ulis, France, 2018; Volume 44.
16. Zhao, B.; Zhang, Y.; Li, X.; Yang, X.; Huang, D. Comparison of indoor aerosol particle concentration and deposition in different ventilated rooms by numerical method. *Build. Environ.* **2004**, *39*, 1–8. [[CrossRef](#)]
17. Breum, N.O.; Skotte, J. Displacement ventilation in industry—A design principle for improved air quality. *Build. Environ.* **1992**, *27*, 447–453. [[CrossRef](#)]
18. Habchi, C.; Ghali, K.; Ghaddar, N. A simplified mathematical model for predicting cross contamination in displacement ventilation air-conditioned spaces. *Aerosol Sci.* **2014**, *76*, 72–86. [[CrossRef](#)]
19. Lin, Z.; Chow, T.; Fong, K.; Wang, Q.; Li, Y. Comparison of performances of displacement and mixing ventilations. Part I: Thermal comfort. *Int. J. Refrig.* **2005**, *28*, 276–287. [[CrossRef](#)]
20. Zhang, J.; Long, Z.; Liu, W.; Chen, Q. Strategy for Studying Ventilation Performance in Factories. *Aerosol Air Qual. Res.* **2016**, *16*, 442–452. [[CrossRef](#)]
21. Mundt, E. *The Performance of Displacement Ventilation Systems: Experimental and Theoretical Studies*; Bulletin No. 38; Royal Institute of Technology, Building Services Engineering: Stockholm, Sweden, 1996.
22. Niemela, R.; Koskela, H.; Engstrom, K. Stratification of welding fumes and grinding particles in a large factory hall equipped with displacement ventilation. *Ann. Occup. Hyg.* **2001**, *45*, 467–471. [[CrossRef](#)]
23. Wei, G.; Chen, B.; Lai, D.; Chen, Q. An improved displacement ventilation system for a machining plant. *Atmos. Environ.* **2020**, *228*, 117419. [[CrossRef](#)]
24. Wang, J.; Huo, Q.; Zhang, T.; Liu, F.; Wang, S.; Ma, Z.; Jiang, S. Performance evaluation for a coupled push–pull ventilation and air curtain system to restrict pollutant dispersion in a factory building. *J. Build. Eng.* **2021**, *43*, 103164. [[CrossRef](#)]
25. Zhao, J.; Liu, Y.; Li, X.; Xu, W.; Wang, H. Numerical investigation on ventilation control strategy of reducing circulating air volume in a factory for storing satellites. *Energy Build.* **2021**, *252*, 111444. [[CrossRef](#)]
26. Lin, Y.J.P.; Lin, C.L. A study on flow stratification in a space using displacement ventilation. *Int. J. Heat Mass Transf.* **2014**, *73*, 67–75. [[CrossRef](#)]
27. Lin, Y.; Wu, J.Y. A study on density stratification by mechanical extraction displacement ventilation. *Int. J. Heat Mass Transf.* **2017**, *110*, 447–459. [[CrossRef](#)]
28. Wang, H.-Q.; Huang, C.-H.; Liu, D.; Zhao, F.; Sun, H.; Wang, F.-F.; Li, C.; Kou, G.; Ye, M. Fume transports in a high rise industrial welding hall with displacement ventilation system and individual ventilation units. *Build. Environ.* **2012**, *52*, 119–128. [[CrossRef](#)]
29. Sutherland, J.; Kulur, V.; King, N.; von Turkovich, B. An Experimental Investigation of Air Quality in Wet and Dry Turning. *CIRP Ann.* **2000**, *49*, 61–64. [[CrossRef](#)]
30. Wang, X.; Zhou, Y.; Wang, F.; Jiang, X.; Yang, Y. Exposure levels of oil mist particles under different ventilation strategies in industrial workshops. *Build. Environ.* **2021**, *206*, 108264. [[CrossRef](#)]
31. Kam, W.; Cheung, K.; Daher, N.; Sioutas, C. Particulate matter (PM) concentrations in underground and ground-level rail systems of the Los Angeles Metro. *Atmos. Environ.* **2011**, *45*, 1506–1516. [[CrossRef](#)]
32. Li, Z.; Che, W.; Lau, A.K.; Fung, J.C.; Lin, C.; Lu, X. A feasible experimental framework for field calibration of portable light-scattering aerosol monitors: Case of TSI DustTrak. *Environ. Pollut.* **2019**, *255*, 113136. [[CrossRef](#)]
33. Zhang, Z.; Chen, Q. Prediction of particle deposition onto indoor surfaces by CFD with a modified Lagrangian method. *Atmos. Environ.* **2009**, *43*, 319–328. [[CrossRef](#)]
34. Hinds, W.; Zhu, Y. *Aerosol Technology: Properties, Behavior, and Measurement of Airborne Particles*; Wiley: Hoboken, NJ, USA, 1982.
35. Zhang, Z.; Chen, Q. Experimental measurements and numerical simulations of particle transport and distribution in ventilated rooms. *Atmos. Environ.* **2006**, *40*, 3396–3408. [[CrossRef](#)]
36. Patankar, S.V.; Spalding, D. A calculation procedure for heat, mass and momentum transfer in three-dimensional parabolic flows. *Int. J. Heat Mass Transf.* **1972**, *15*, 1787–1806. [[CrossRef](#)]
37. Rohdin, P.; Moshfegh, B. Environment. Numerical predictions of indoor climate in large industrial premises. A comparison between different $k-\epsilon$ models supported by field measurements. *Build. Environ.* **2007**, *42*, 3872–3882. [[CrossRef](#)]
38. Zhang, Z.; Chen, Q. Comparison of the Eulerian and Lagrangian methods for predicting particle transport in enclosed spaces. *Atmospheric Environ.* **2007**, *41*, 5236–5248. [[CrossRef](#)]
39. Huang, C.-H.; Lin, P.-Y. Influence of spatial layout on airflow field and particle distribution on the workspace of a factory. *Build. Environ.* **2014**, *71*, 212–222. [[CrossRef](#)]
40. China Nonferrous Metals Industry Association. *Design Code for Heating Ventilation and Air Conditioning of Industrial Buildings—GB50019*; China Building Industry Press: Beijing, China, 2015.
41. Iwasaki, M.; Hirai, K.; Fukumori, K.; Higashi, H.; Inomata, Y.; Seto, T. Characterization of Submicron Oil Mist Particles Generated by Metal Machining Processes. *Aerosol Air Qual. Res.* **2020**, *20*, 1469–1479. [[CrossRef](#)]
42. Jia, X.; Liu, D.; Liu, C. Simulation study of displacement ventilation in a closed welding workshop. *J. HAVC* **2010**, *40*, 76–80.
43. Chen, J.; Zhao, B.; Li, X. Numerical study of particle distribution under different air volumes of displacement ventilation. In *Proceedings of the National HVAC Refrigeration Annual Conference*; London, UK, 2004; p. 102.

44. Maupins, K.; Hitchings, D.T. Reducing employee exposure potential using the ANSI/ASHRAE 110 Method of Testing Performance of Laboratory Fume Hoods as a diagnostic tool. *Am. Ind. Hyg. Assoc. J.* **1998**, *59*, 133–138. [[CrossRef](#)] [[PubMed](#)]
45. Shi, Z.; Lu, Z.; Chen, Q. Indoor airflow and contaminant transport in a room with coupled displacement ventilation and passive-chilled-beam systems. *Build. Environ.* **2019**, *161*, 106244. [[CrossRef](#)]

Disclaimer/Publisher's Note: The statements, opinions and data contained in all publications are solely those of the individual author(s) and contributor(s) and not of MDPI and/or the editor(s). MDPI and/or the editor(s) disclaim responsibility for any injury to people or property resulting from any ideas, methods, instructions or products referred to in the content.